Extended Skyrme interaction in the microscopic optical model of nucleon-nucleus scattering

V. V. Pilipenko* and V. I. Kuprikov

National Science Center "Kharkov Institute of Physics and Technology", 1 Akademichna Street, Kharkov 61108, Ukraine

(Received 9 October 2012; published 27 December 2012)

The microscopic optical potential model based on calculations of the mass operator of the single-particle Green function has been refined by using the extended Skyrme-force variant, which involves additional both density- and momentum-dependent terms, and is employed for describing simultaneously properties of nuclei, nuclear-matter characteristics, and the nucleon-nucleus scattering observables in a self-consistent approach. From analyzing a differential cross section and polarization for a chosen case of the elastic neutron-nucleus scattering while controlling the characteristics of nuclear matter and finite-nuclei structure, a few sets of parameters have been determined for new variants of the extended Skyrme forces. It has been shown that the allowance for both the density- and momentum-dependent terms makes it possible to significantly improve the agreement with experimental data. The proposed extended Skyrme-force variants provide a satisfactory description for cross sections and analyzing powers of the neutron and proton scattering in a wide range of the target-nucleus mass numbers at different incident nucleon energies, as well as for a variety of nuclear structure characteristics.

DOI: 10.1103/PhysRevC.86.064613 PACS number(s): 24.10.Ht, 21.30.Fe, 21.60.Jz

I. INTRODUCTION

Starting from Ref. [1], extensive investigations have been devoted to the elaboration of effective nucleon-nucleon (*NN*) forces of the Skyrme type [2], which are widely used in microscopic calculations of nuclear structure and properties of nuclear matter. At the present time, in the literature (see, for example, Refs. [3–5]) much attention is given to the problem of searching for effective *NN* forces which could be simultaneously applicable for describing the ground-state and spectroscopic properties of nuclei, in particular, of exotic ones, the properties of excited states of nuclei, including giant resonances, and for astrophysical problems, such as calculations of neutron stars. The methods of determining parameters of these forces are being refined and generalizations are being considered, which make their form more flexible. On this basis, it is of interest to extend the field of application of the Skyrme forces to the description of nuclear scattering processes. In this article, the authors continue their previous investigations [6–8] of the nucleon-nucleus (*NA*) scattering at medium energies on the basis of the model of microscopic optical potential (MOP) with using the density-dependent Skyrme *NN* forces.

The *NA* MOP model under consideration is based on approximate calculations of the mass operator of the one-particle Green function. In Ref. [6], the real and imaginary parts of the sought MOP were calculated in the nuclear-matter and local-density approximations by perturbation theory up to the second order on the basis of the Skyrme *NN* forces. This approach is close to the method used in Refs. [9,10]. In Refs. [7,8], this model was refined by using the Hartree-Fock (HF) potential for finite nuclei as the real part of the MOP, as well as by adding the spin-orbit potential. An important distinction of our studies in Refs. [6–8] is the fact that in them we employed self-consistent calculations of the *NA* MOP and the nucleon densities of target nuclei, while in Refs. [9,10] phenomenological nucleon densities were used. In Refs. [7,8], a revision of the parameters of the standard-form Skyrme forces was carried out based on the proposed procedure of analyzing differential cross sections of the elastic neutron-nucleus (nA) scattering with the simultaneous control of certain characteristics of nuclear structure. In those papers, it was noted that some problems arising in the description of the differential cross sections in the region of large scattering angles with the neutron energy increase might indicate that it was necessary to improve the model for the imaginary part of the MOP, and probably also to use a more sophisticated model of the Skyrme forces. In this connection, it should be emphasized that at present some possible modifications of the form of Skyrme *NN* forces are discussed in the literature with the aim to improve the description of different characteristic properties of nuclear structure and also to refine the neutron-star models. One such modification is the inclusion of terms depending on both the nuclear density and the relative momentum of the interacting nucleons [11–14] or alternatively of terms corresponding to the momentum-dependent three-particle forces [15].

In this article, the *NA* MOP model considered by us is also improved by making use of the extended variant of Skyrme forces that involves both the density- and momentum-dependent terms. The allowance for such terms in the Skyrme forces is of interest for constructing the *NA* MOP because they can yield important contributions to the surface region of the imaginary part of the optical potential, which should have an essential effect on the behavior of observables of the *NA* scattering. Note that in the aforementioned Ref. [10] the *NA* scattering cross sections were described using the GS2 force from Ref. [11], which involves some of the terms of this type.

In view of the fact that in Refs. [7,8] we succeeded in finding variants of the standard-form Skyrme forces that provided promising results for describing the *NA* scattering observables, here we carry out a search for new variants of the extended Skyrme forces of the type being considered. We employ a procedure of optimizing the *NN* force parameters

*vpilipenko@kipt.kharkov.ua

to ensure a satisfactory description of angular distributions of the elastic nA scattering cross sections and polarizations and, simultaneously, of characteristics of nuclei and nuclear matter. In doing this, a wider set of the characteristics of nuclear matter and finite-nuclei structure are controlled than as was done in Refs. [7,8]. Further, we use the found variants of the extended Skyrme forces for calculations of cross sections and polarization characteristics of the elastic nA and proton-nucleus (pA) scattering.

II. THE *NA* MOP MODEL WITH THE EXTENDED SKYRME INTERACTION

In the *NA* MOP model under consideration and in calculating the nuclear structure characteristics, we make use of the extended variant of Skyrme interaction determined as follows:

$$V_{\rm Sk} = v_{c1}(\mathbf{r}) + v_{c2}(\mathbf{r}, \rho) + v_{\rm so}(\mathbf{r}). \tag{1}$$

Here the central density-independent part of *NN* force has the conventional form

$$\begin{aligned} v_{c1}(\mathbf{r}) = {} & t_0(1 + x_0 P_\sigma)\delta(\mathbf{r}) \\ & + \tfrac{1}{2}t_1(1 + x_1 P_\sigma)[\mathbf{k}'^2\delta(\mathbf{r}) + \delta(\mathbf{r})\mathbf{k}^2] \\ & + t_2(1 + x_2 P_\sigma)\mathbf{k}'\delta(\mathbf{r})\mathbf{k}, \end{aligned} \tag{2}$$

and for the density-dependent part of the interaction we use the following extended expression:

$$\begin{aligned} v_{c2}(\mathbf{r}, \rho) = {} & \tfrac{1}{6}t_3(1 + x_3 P_\sigma)\rho^\gamma(\mathbf{R})\delta(\mathbf{r}) + \tfrac{1}{2}t_4(1 + x_4 P_\sigma) \\ & \times [\mathbf{k}'^2\rho^{\gamma_4}(\mathbf{R})\delta(\mathbf{r}) + \delta(\mathbf{r})\rho^{\gamma_4}(\mathbf{R})\mathbf{k}^2] \\ & + t_5(1 + x_5 P_\sigma)\mathbf{k}'\rho^{\gamma_5}(\mathbf{R})\delta(\mathbf{r})\mathbf{k}. \end{aligned} \tag{3}$$

In Eqs. (2) and (3), the conventional notation is used: $\mathbf{r} = \mathbf{r}_1 - \mathbf{r}_2$ and $\mathbf{R} = (\mathbf{r}_1 + \mathbf{r}_2)/2$ are the relative and center-of-mass radius vectors of the interacting nucleons; $\rho = \rho_n + \rho_p$, ρ_n, and ρ_p are the total, neutron, and proton densities of the target nucleus; $\mathbf{k} = -i\partial/\partial\mathbf{r}$ and $\mathbf{k}' = i\partial/\partial\mathbf{r}'$ are the momentum operators of the relative motion of the nucleons in the initial and final states, respectively; P_σ is the operator of the nucleon spin permutation. Formula (3), in distinction to the standard-form Skyrme forces [1,2], which involve only the first term from Eq. (3), additionally contains both density- and momentum-dependent terms (the second and third ones) in the same form, as was used in Refs. [13,14]. The spin-orbit part of the *NN* forces has the standard form [1,2]

$$v_{\rm so}(\mathbf{r}) = i W_0(\boldsymbol{\sigma}_1 + \boldsymbol{\sigma}_2)[\mathbf{k}' \times \delta(\mathbf{r})\mathbf{k}]. \tag{4}$$

The *NN* interaction under consideration is characterized by the phenomenological parameters t_n, x_n ($n = 0$–5), and W_0. Note that for the both density- and momentum-dependent terms, whose magnitude is determined by the parameters t_4, t_5, x_4, and x_5, arbitrary density exponents γ_4 and γ_5 are allowed, which in the general case are different from the exponent γ in the standard density-dependent term.

The optical potential describing the *NA* scattering is found from calculations of the mass operator of the one-particle Green function by perturbation theory up to the Goldstone diagrams of the second order, inclusive (see Refs. [8,10]). Using the transformation from the nonlocal Skyrme-Hartree-Fock equation to its local form [16], it is possible to represent the *NA* MOP for incident nucleons of sort q ($q = \pm 1 \equiv n, p$) in the following form:

$$\begin{aligned} U_q(\mathbf{r}, E) = {} & V_q(r, E) + \frac{1}{r}V_{{\rm SO},q}(r)(\mathbf{l}\cdot\boldsymbol{\sigma}) \\ & + i W_q(r, E) + \delta_{q,p}\frac{m_q^*(r)}{m_q}V_C(r). \end{aligned} \tag{5}$$

In Eq. (5), the central real part of the energy-dependent local potential is given by the formula

$$\begin{aligned} V_q(r, E) = {} & \frac{m_q^*}{m_q}[V^{\rm (HF)}(r) + V^{(m)}(r)]_q \\ & + \left(1 - \frac{m_q^*(r)}{m_q}\right)\frac{M}{M + m_q}E. \end{aligned} \tag{6}$$

Here E is the laboratory energy, m_q and M are the incident-nucleon and target-nucleus masses, and the effective incident-nucleon mass m_q^* in the nucleus is defined according to the expression

$$\begin{aligned} \frac{m_q}{m_q^*} = {} & 1 + \frac{2m_q}{\hbar^2}\frac{1}{4}[\rho(g_1 + g_2 + g_4\rho^{\gamma_4} + g_5\rho^{\gamma_5}) \\ & + \rho_q(-h_1 + h_2 - h_4\rho^{\gamma_4} + h_5\rho^{\gamma_5})]. \end{aligned} \tag{7}$$

In Eq. (7) and below, we use the notation for such Skyrme-parameter combinations: $g_i = t_i(1 + \frac{1}{2}x_i)$, $h_i = t_i(\frac{1}{2} + x_i)$. In Eq. (6), the quantity $V^{\rm (HF)}$ corresponds to the HF potential for finite nuclei with allowance for the rearrangement potential [1], which arises owing to the density dependence of the *NN* forces, and is determined by the following expression (see also Ref. [13]):

$$\begin{aligned} V^{\rm (HF)} = {} & \rho g_0 - \rho_q h_0 + \frac{1}{4}(g_1 + g_2 + g_4\rho^{\gamma_4} + g_5\rho^{\gamma_5})\tau + \frac{1}{4}(-h_1 + h_2 - h_4\rho^{\gamma_4} + h_5\rho^{\gamma_5})\tau_q \\ & + \frac{1}{6}\rho^\gamma(\rho g_3 - \rho_q h_3) + \frac{1}{12}\gamma\rho^{\gamma-1}\left[\rho^2 g_3 - \left(\rho_n^2 + \rho_p^2\right)h_3\right] + \frac{1}{4}(g_4\rho^{\gamma_4} + g_5\rho^{\gamma_5})\tau \\ & + \frac{1}{4}(-h_4\rho^{\gamma_4 - 1} + h_5\rho^{\gamma_5 - 1})(\rho_n\tau_n + \rho_p\tau_p) + \frac{1}{8}[-3g_1 + g_2 - (3 + 2\gamma_4)g_4\rho^{\gamma_4} + g_5\rho^{\gamma_5}]\Delta\rho \\ & + \frac{1}{8}(3h_1 + h_2 + 3h_4\rho^{\gamma_4} + h_5\rho^{\gamma_5})\Delta\rho_q + \frac{1}{16}[-(3 + 2\gamma_4)\gamma_4 g_4\rho^{\gamma_4 - 1} + \gamma_5 g_5\rho^{\gamma_5 - 1}](\nabla\rho)^2 \\ & + \frac{1}{8}\gamma_4 h_4\rho^{\gamma_4 - 1}(\rho_q\Delta\rho + \rho_n\Delta\rho_n + \rho_p\Delta\rho_p) + \frac{1}{8}(3\gamma_4 h_4\rho^{\gamma_4 - 1} + \gamma_5 h_5\rho^{\gamma_5 - 1})(\nabla\rho\cdot\nabla\rho_q) \end{aligned}$$

$$-\frac{1}{16}(\gamma_4 h_4\rho^{\gamma_4-1}+\gamma_5 h_5\rho^{\gamma_5-1})[(\nabla\rho_n)^2+(\nabla\rho_p)^2]+\frac{1}{8}\gamma_4(\gamma_4-1)h_4\rho^{\gamma_4-2}\rho_q(\nabla\rho)^2$$
$$-\frac{1}{16}(\gamma_4 t_4 x_4\rho^{\gamma_4-1}+\gamma_5 t_5 x_5\rho^{\gamma_5-1})J^2+\frac{1}{16}(\gamma_4 t_4\rho^{\gamma_4-1}-\gamma_5 t_5\rho^{\gamma_5-1})\left(J_n^2+J_p^2\right)-\frac{1}{2}W_0\left[\frac{2}{r}(J+J_q)+\frac{d}{dr}(J+J_q)\right]. \quad (8)$$

In Eq. (8), τ_q is the kinetic-energy density of nucleons of sort q, $\tau=\tau_n+\tau_p$, and the functions $J_q(r)$ and $J(r)=J_n(r)+J_p(r)$ are the spin-orbit nucleon densities [1]. These quantities together with the nucleon densities $\rho_q(r)$ and $\rho(r)$ are found from the self-consistent calculations (see Refs. [1,17]) of the target nucleus structure by solving the HF equations allowing for the nucleon pairing in the BCS approximation with the constant pairing forces $G_{p,n}=19.5[1\pm 0.51(N-Z)/A]/A$ (in MeV) [18]. In the calculations, we take into account the direct and exchange parts of the Coulomb potential:

$$V_C(r)=e^2\int\frac{\rho_p(r')}{|\mathbf{r}-\mathbf{r}'|}d\mathbf{r}'-e^2\left(\frac{3}{\pi}\right)^{1/3}\rho_p^{1/3}(r). \quad (9)$$

When solving the HF equation, we allow for the c.m. motion in a traditional way [1] by introducing the factor $(A-1)/A$ in the kinetic-energy term.

The term $V^{(m)}(r)$ in Eq. (6) arises in the transformation from the nonlocal HF equation to the Schrödinger equation with energy-dependent local potential owing to the dependence of the effective incident-nucleon mass on the radius and has the form [16]

$$V^{(m)}(r)=\frac{1}{2}\Delta\frac{\hbar^2}{2m_q^*(r)}-\frac{m_q^*(r)}{2\hbar^2}\left[\frac{d}{dr}\frac{\hbar^2}{2m_q^*(r)}\right]^2. \quad (10)$$

We take the real spin-orbit potential in Eq. (5) in the form that corresponds to the HF theory of finite nuclei with the Skyrme interaction (1)–(3)

$$V_{\mathrm{SO},q}(r)=\frac{m_q^*(r)}{m_q}\left\{\frac{1}{2}W_0\frac{d}{dr}[\rho(r)+\rho_q(r)]+\frac{1}{8}(t_1-t_2+t_4\rho^{\gamma_4}-t_5\rho^{\gamma_5})J_q(r)-\frac{1}{8}(t_1x_1+t_2x_2+t_4x_4\rho^{\gamma_4}+t_5x_5\rho^{\gamma_5})J(r)\right\}. \quad (11)$$

The imaginary part of the MOP $W_q(r,E)$ is calculated with the *NN* interaction (1)–(3) in the nuclear-matter and local-density approximations analogously to the approach described in detail in Refs. [6–10] and it is defined by the following formulas:

$$W_q(r,E)=-\frac{1}{64\pi^5}\sum_{i=1}^{7}W_i, \quad (12)$$

$$W_1=\left(2g_{00}+\frac{2}{3}g_{03}\rho^{\gamma}+\frac{1}{18}g_{33}\rho^{2\gamma}\right)[I_1(q,n)+I_1(q,p)]-\left(2h_{00}+\frac{2}{3}h_{03}\rho^{\gamma}+\frac{1}{18}h_{33}\rho^{2\gamma}\right)I_1(q,q), \quad (13)$$

$$W_2=\left[2(g_{01}+g_{04}\rho^{\gamma_4})+\frac{1}{3}\rho^{\gamma}(g_{13}+g_{34}\rho^{\gamma_4})\right]\times[I_2(q,n)+I_2(q,p)]-[2(h_{01}+h_{04}\rho^{\gamma_4})+\frac{1}{3}\rho^{\gamma}(h_{13}+h_{34}\rho^{\gamma_4})]I_2(q,q), \quad (14)$$

$$W_3=\frac{1}{2}(g_{11}+2g_{14}\rho^{\gamma_4}+g_{44}\rho^{2\gamma_4})[I_3(q,n)+I_3(q,p)]-\frac{1}{2}(h_{11}+2h_{14}\rho^{\gamma_4}+h_{44}\rho^{2\gamma_4})I_3(q,q), \quad (15)$$

$$W_4=2[2(g_{02}+g_{05}\rho^{\gamma_5})+\frac{1}{3}\rho^{\gamma}(g_{23}+g_{35}\rho^{\gamma_5})]\times[I_4(q,n)+I_4(q,p)], \quad (16)$$

$$W_5=2(g_{12}+g_{24}\rho^{\gamma_4}+g_{15}\rho^{\gamma_5}+g_{45}\rho^{\gamma_4+\gamma_5})\times[I_5(q,n)+I_5(q,p)], \quad (17)$$

$$W_6=2(g_{22}+2g_{25}\rho^{\gamma_5}+g_{55}\rho^{2\gamma_5})[I_6(q,n)+I_6(q,p)]+2(h_{22}+2h_{25}\rho^{\gamma_5}+h_{55}\rho^{2\gamma_5})I_6(q,q), \quad (18)$$

$$W_7=4W_0^2[I_7(q,n)+I_7(q,p)+I_7(q,q)]. \quad (19)$$

Here the notation is used: $g_{ij}=t_it_j[1+x_ix_j+(x_i+x_j)/2]$, $h_{ij}=t_it_j[x_i+x_j+(1+x_ix_j)/2]$. The quantities $I_l(q,q_\mu)$ are integrals over the momenta of intermediate nucleon states, which arise in the calculations of the imaginary part of MOP from the second-order diagrams, and their form is considered in Refs. [7,9]. The integrals $I_l(q,q_\mu)$ depend on the magnitude of the incident-nucleon wave vector k_α being related to the nucleon energy E in the laboratory frame by the dispersion law

$$k_\alpha^2=\frac{2m_q^*}{\hbar^2}\left[\frac{ME}{M+m_q}-V^{(\mathrm{HF})}-\delta_{q,p}V_C\right]. \quad (20)$$

It should be noted that, since the potential $V^{(\mathrm{HF})}$ contains the rearrangement potential, the latter essentially affects the magnitude of the imaginary part of MOP through the dispersion law (20), as it was discussed in detail in Ref. [6].

To demonstrate the results given by the described model, in Figs. 1 and 2 we present examples of calculations of the differential cross section $\sigma(\theta)\equiv d\sigma(\theta)/d\Omega$ and analyzing power $A_y(\theta)$ for the elastic scattering of 13.9-MeV neutrons by ^{120}Sn nuclei, which we have carried out with different known variants of the Skyrme forces. The results of calculations with the standard-form *NN* forces KDE0 [19], SV-mas07 [20], BSk17 [13], and SkOP2 [8] are shown in Fig. 1. We stress that the variant SkOP2 was obtained by us from the Skyrme-parameter optimization by analyzing the differential cross section of the elastic $n+{}^{116}$Sn scattering at the same energy of 13.9 MeV. As can be seen from the figure, the SkOP2 force provides a significantly better description of the nA scattering experimental data from Ref. [21]. However, there are some discrepancies with the data at large scattering angles, which worsen when the incident neutron energy increases

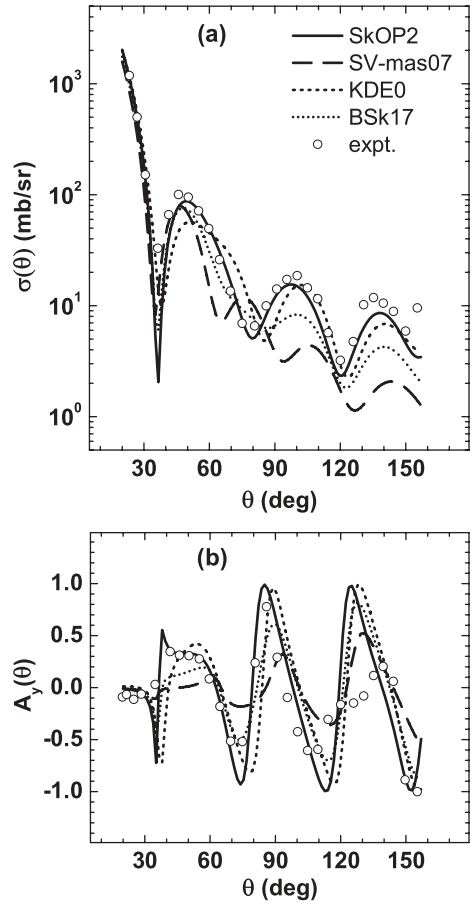

FIG. 1. Differential cross section $\sigma(\theta)$ (a) and analyzing power $A_y(\theta)$ (b) of the elastic scattering of 13.9-MeV neutrons on ^{120}Sn nuclei calculated with different standard-form Skyrme forces.

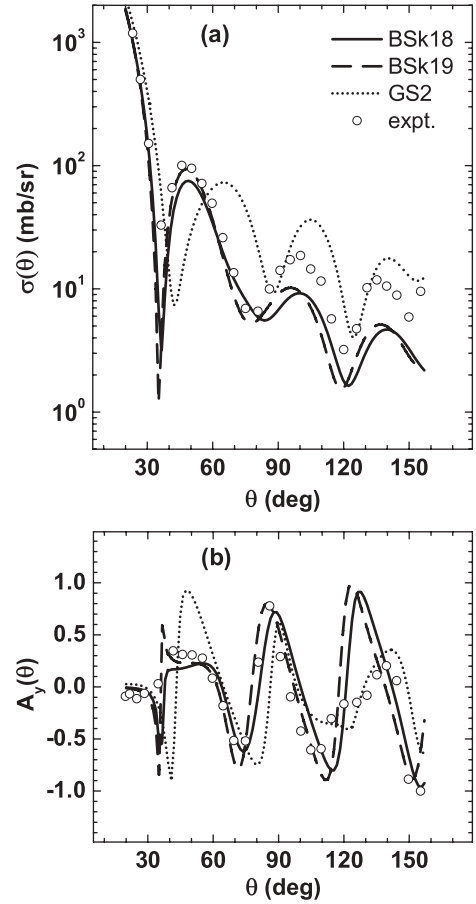

FIG. 2. The same as in Fig. 1, but calculated with different extended Skyrme forces.

(see Ref. [8]). For this reason, it is interesting to investigate whether the situation could be improved by using the extended Skyrme-force model under consideration. In Fig. 2, we show the results obtained with these types of Skyrme forces GS2 [11], BSk18 [13], and BSk19 [14]. We have also performed calculations with the forces BSk20 and BSk21 from Ref. [14], which yield results very close to those for BSk19 and, therefore, we do not present them here. Note that the GS2 force does not yield an acceptable agreement with the experimental *NA* scattering observables [21]. It should be mentioned that in Ref. [10] the calculations with GS2 gave a better description of *NA* scattering cross sections, but in Ref. [10] the rearrangement potential was not taken into account and, besides, phenomenological nuclear densities were used, i.e., the self-consistent calculations of the nuclear structure were not carried out. Our calculations with the BSk forces give a reasonable description of the data at not very large scattering angles, but the agreement with the experiment worsens when the scattering angle increases. For this reason, as well as taking into account the considerable spread of the calculation results for different Skyrme forces, it is appropriate to optimize the extended-Skyrme-force parameters to improve the description of *NA* scattering by using a procedure analogous to that employed in Ref. [8].

III. PROCEDURE OF OPTIMIZING THE EXTENDED-SKYRME-FORCE PARAMETERS

Let us consider the procedure we use for determining values of the parameters of the extended variant of Skyrme *NN* forces (1)–(3), which would be applicable for a satisfactory description of the characteristics of nuclear matter and structure of finite nuclei, as well as of the *NA* scattering observables on the basis of the considered model of *NA* MOP. An analogous problem of improving the parameters of the standard-form Skyrme forces was considered by us in Refs. [7,8] with the help of the optimization procedure proposed in those papers. Here we perform a search for new extended variants of the *NN* forces using a similar procedure.

As in the approach used in Refs. [7,8], the procedure of optimizing the parameters of the extended *NN* forces includes a fitting of observables of the elastic neutron scattering on a chosen target nucleus at a certain energy on the basis of the considered model of *NA* MOP while controlling the characteristics of symmetric nuclear matter. The correct description of the parameters of symmetric ($\rho_n = \rho_p = \rho/2 =$ const) nuclear matter is a usual requirement in determining Skyrme-force parameters. The set of controlled characteristics of nuclear matter, as it also was in Refs. [7,8], includes the average binding energy per nucleon E/A, the equilibrium density ρ_0, the effective nucleon mass in nuclear matter m^*,

and the symmetry energy J. In distinction to Refs. [7,8], to these quantities are added the enhancement factor of the Thomas-Reiche-Kuhn energy-weighted sum rule κ for the isovector giant dipole resonance, which is related to the isovector effective nucleon mass $m/m_v^* = 1 + \kappa$, as well as the incompressibility coefficient of the nuclear matter K_v. Note that the expressions we use for these quantities as functions of the parameters of the extended Skyrme forces (1)–(3) coincide with those presented in Refs. [5,13], and therefore we do not give them here. At the present time, for the aforementioned nuclear-matter parameters there are certain estimates of their acceptable numerical values, and therefore, when optimizing the *NN* force parameters, we do not allow them to deviate too widely from these values. For this purpose, we include these quantities in the set of independently varied parameters together with the Skyrme parameters t_2, x_2, x_3, W_0, t_5, x_4, and x_5, while other *NN* force parameters t_0, t_1, t_3, x_0, x_1, and t_4 are calculated through the chosen independent quantities according to the following formulas:

$$t_4 = \frac{1}{3}\rho_0^{-\gamma_4} C_m^4, \tag{21}$$

$$t_3 = -\frac{16}{\gamma\rho_0^{\gamma+1}}\left[E/A + \tfrac{1}{5}(2m/m^* - 3)\frac{\hbar^2}{2m}k_F^2 + \tfrac{3}{80}\left(\gamma_4 C_m^4 + \gamma_5 C_m^5\right)\rho_0 k_F^2\right], \tag{22}$$

$$t_0 = \frac{8}{3\rho_0}\left[E/A - \frac{3}{5}m/m^*\frac{\hbar^2}{2m}k_F^2 - \frac{1}{16}t_3\rho_0^{\gamma+1}\right], \tag{23}$$

$$t_1 = \frac{1}{3}\left[C_m - 5t_2\left(1 + \frac{4}{5}x_2\right)\right], \tag{24}$$

$$x_0 = \frac{4}{t_0\rho_0}\left\{\frac{1}{3}\frac{\hbar^2}{2m}k_F^2 - J - \frac{1}{8}\left[t_0 + \frac{1}{3}t_3\left(\frac{1}{2} + x_3\right)\rho_0^{\gamma}\right]\rho_0 - \frac{1}{8}t_1x_1\rho_0 k_F^2 + \frac{1}{6}t_2\left(1 + \frac{5}{4}x_2\right)\rho_0 k_F^2 - \frac{1}{24}\left[C_m^4 x_4 - 5t_5\left(\frac{4}{5} + x_5\right)\rho_0^{\gamma_5}\right]\rho_0 k_F^2\right\}, \tag{25}$$

$$x_1 = \frac{1}{t_1}\left\{8\frac{\hbar^2}{2m}\frac{\kappa}{\rho_0} - t_2(2 + x_2) - t_4(2 + x_4)\rho_0^{\gamma_4} - t_5(2 + x_5)\rho_0^{\gamma_5}\right\} - 2. \tag{26}$$

In Eqs. (21)–(26), $k_F = (3\pi^2\rho_0/2)^{1/3}$ is the nucleon Fermi momentum, and the following notations are used:

$$C_m^5 = 5t_5(1 + 4x_5/5)\rho_0^{\gamma_5}, \tag{27}$$

$$C_m^4 = \frac{80}{9\gamma_4(3\gamma_4 - 3\gamma + 4)\rho_0 k_F^2}\left\{9(\gamma + 1)E/A - \frac{3}{5}[(2 - 3\gamma)(2m/m^* - 3) + 3]\frac{\hbar^2}{2m}k_F^2 - \frac{9}{80}\gamma_5(3\gamma_5 - 3\gamma + 4)C_m^5\rho_0 k_F^2 + K_v\right\}, \tag{28}$$

$$C_m = -\frac{16}{3\rho_0 k_F^2}\left\{\frac{6}{5}\frac{\hbar^2}{2m}k_F^2 + \frac{9}{8}t_0\rho_0 + \frac{3}{16}(\gamma + 1)t_3\rho_0^{\gamma+1} + \frac{3}{80}\left[(3\gamma_4 + 5)C_m^4 + (3\gamma_5 + 5)C_m^5\right]\rho_0 k_F^2\right\}. \tag{29}$$

When optimizing the parameters of the Skyrme forces under consideration, as distinct from Refs. [7,8], the fitting was performed not only for the differential cross section but also for the corresponding analyzing power for the chosen case of elastic *NA* scattering. Specifically in this work, for the analysis we have chosen the experimental data on the elastic scattering of neutrons on ^{120}Sn at the energy of 13.9 MeV from Ref. [21]. When fitting the scattering observables, we also controlled the binding energies and charge rms radii of the target nucleus (as was done also in Refs. [7,8]) and additionally of two more nuclei, namely, ^{40}Ca and ^{208}Pb, in order to improve the description of these characteristics of nuclei in a wide range of the mass numbers. Besides, we also controlled the spin-orbit splitting energy for the neutron $3p_{1/2}$ and $3p_{3/2}$ levels for the ^{208}Pb nucleus. Therefore, the following modified $\tilde{\chi}^2$ value was minimized in the fitting:

$$\tilde{\chi}^2 = \frac{1}{N_{\sigma,\mathrm{ex}} - N_{\mathrm{par}}}\sum_{i=1}^{N_{\sigma,\mathrm{ex}}}\left[\frac{\sigma(\theta_i) - \sigma_{\mathrm{ex}}(\theta_i)}{\Delta\sigma_{\mathrm{ex}}^{(i)}}\right]^2 + \frac{1}{N_{A,\mathrm{ex}}}\sum_{i=1}^{N_{A,\mathrm{ex}}}\left[\frac{A_y(\theta_i) - A_{y,\mathrm{ex}}(\theta_i)}{\Delta A_{y,\mathrm{ex}}^{(i)}}\right]^2 + \sum_{n=1}^{3}\left[\left(\frac{E_b^{(n)} - E_{b,\mathrm{ex}}^{(n)}}{\Delta E_b}\right)^2 + \left(\frac{r_{\mathrm{ch}}^{(n)} - r_{\mathrm{ch,ex}}^{(n)}}{\Delta r_{\mathrm{ch}}}\right)^2\right] + \left(\frac{\varepsilon_{\mathrm{so}} - \varepsilon_{\mathrm{so,ex}}}{\Delta\varepsilon_{\mathrm{so}}}\right)^2. \tag{30}$$

Here the first two terms are the χ^2 values for the fitted scattering observables; $\sigma(\theta_i)$, $\sigma_{\mathrm{ex}}(\theta_i)$, $A_y(\theta_i)$, and $A_{y,\mathrm{ex}}(\theta_i)$ are the theoretical and experimental values of the cross section and analyzing power; $\Delta\sigma_{\mathrm{ex}}^{(i)}$ and $\Delta A_{y,\mathrm{ex}}^{(i)}$ are the values of their experimental errors; $N_{\sigma,\mathrm{ex}}$, $N_{A,\mathrm{ex}}$, and N_{par} are the corresponding numbers of experimental points and the number of fitted parameters. Equation (30) also involves the magnitudes of deviations of the calculated binding energies $E_b^{(n)}$ and charge radii $r_{\mathrm{ch}}^{(n)}$ for three chosen nuclei (^{40}Ca, ^{120}Sn, and ^{208}Pb) and aforementioned spin-orbit splitting energy $\varepsilon_{\mathrm{so}}$ from their experimental values $E_{b,\mathrm{ex}}^{(n)}$, $r_{\mathrm{ch,ex}}^{(n)}$, and $\varepsilon_{\mathrm{so,ex}}$ (ΔE_b, Δr_{ch}, and $\Delta\varepsilon_{\mathrm{so}}$ specify the permissible values of these deviations). The calculated charge radii of the nuclei were found with the allowance for the proton and neutron form factors and the spin-orbit correction [22–24].

When searching for new extended *NN* forces, we have considered a variety of their possible variants with different values of the density-dependence exponent $\gamma = \frac{1}{12}, \frac{1}{6}, \frac{1}{3}$, which were used in the literature, and we have also employed different combinations of these values of γ with the following values of two other exponents: $\gamma_4 = \frac{1}{6}, \frac{1}{3}, 1$ and $\gamma_5 = \frac{1}{12}, \frac{1}{6}, \frac{1}{3}, 1$. It should be noted that a number of the variants obtained during the search for the *NN* force parameters yielded results more or less comparable in the quality of describing the experimental

TABLE I. Parameters of the found Skyrme forces.

	SkOP3	SkOP4	SkOP5	SkOP6
t_0 (MeV fm^3)	−1836.14	−1829.89	−1781.69	−3948.54
t_1 (MeV fm^5)	1219.16	1894.98	642.39	990.09
t_2 (MeV fm^5)	−321.93	−515.29	−203.20	−703.29
t_3 (MeV fm$^{3+3\gamma}$)	11935.86	11854.67	11373.99	22094.40
t_4 (MeV fm$^{5+3\gamma_4}$)	−1559.89	−2076.24	−1657.30	−1073.88
t_5 (MeV fm$^{5+3\gamma_5}$)	372.49	593.61	343.30	606.78
x_0	0.5583	0.3390	0.0821	0.6344
x_1	0.8311	0.6276	−0.0664	0.3689
x_2	0.4936	0.4354	0.1184	2.0044
x_3	0.7867	0.4471	−0.0354	0.7898
x_4	1.2343	0.8149	−0.1079	0.7592
x_5	0.9728	0.5015	1.6648	2.9723
W_0 (MeV fm^5)	122.83	125.06	130.76	123.48
γ	1/3	1/3	1/3	1/12
γ_4	1/3	1/6	1	1/3
γ_5	1/3	1/6	1	1/12

data under consideration. Nevertheless, from them we pick out four variants of forces with the exponent values $\gamma = \gamma_4 = \gamma_5 = \frac{1}{3}$ (SkOP3), with $\gamma = \frac{1}{3}$ and $\gamma_4 = \gamma_5 = \frac{1}{6}$ (SkOP4), with $\gamma = \frac{1}{3}$ and $\gamma_4 = \gamma_5 = 1$ (SkOP5), and with $\gamma = \gamma_5 = \frac{1}{12}$ and $\gamma_4 = \frac{1}{3}$ (SkOP6), for which we present the results of calculations below. The parameter values found for these new variants of the extended Skyrme *NN* forces are presented in Table I and the corresponding values of the parameters of nuclear matter are given in Table II.

The results of the optimization analysis of the differential cross section and analyzing power of the elastic $n + {}^{120}$Sn scattering at 13.9 MeV for the four found variants of the extended *NN* forces are shown in Fig. 3. It is seen from Fig. 3 that all *NN* forces found in this work provide a good description of the fitted scattering cross section, especially improving the agreement with the experimental data at large scattering angle, as compared with the results obtained for the standard-form forces SkOP2, which have been shown in Fig. 1. Simultaneously, we have obtained a satisfactory description of the angular distribution of the analyzing power except for the region of very large scattering angles. Note that the best description of the fitted observables is provided by the force variants SkOP3 and SkOP4.

TABLE II. Parameters of nuclear matter for the found Skyrme forces.

	SkOP3	SkOP4	SkOP5	SkOP6
E/A (MeV)	−16.123	−16.016	−16.012	−15.953
ρ_0 (fm^{-3})	0.1585	0.1585	0.1585	0.1586
m^*/m	0.7569	0.7525	0.7599	0.7083
J (MeV)	31.886	30.870	31.851	30.424
L (MeV)	81.0	74.5	79.8	87.1
K_v (MeV)	220.4	222.6	220.9	220.0
K' (MeV)	484.5	454.9	526. 4	412.4
κ	0.495	0.494	0.491	0.491
G_0	−0.024	−0.031	0.020	0.41
G'_0	0.40	0.45	0.36	0.31
G_1	0.52	0.61	0.46	0.48
G'_1	0.54	0.48	0.58	0.60
F_0	−0.24	−0.24	−0.24	−0.29
F'_0	0.98	0.90	0.98	0.77
F_1	−0.73	−0.74	−0.72	−0.88
F'_1	0.39	0.37	0.40	0.17

The found extended Skyrme forces also yield a satisfactory description of the binding energies and charge rms radii not only for the ^{40}Ca, ^{120}Sn, and ^{208}Pb nuclei, which are involved in the optimization procedure, but also for various other medium and heavy nuclei. This is shown in Fig. 4, which presents the relative deviations (in percentages) of the theoretical values from the experimental data [25,26] for binding energies, $\delta E_b = (E_{b,\mathrm{ex}} - E_{b,\mathrm{th}})/E_{b,\mathrm{ex}}$, and charge radii, $\delta r_{\mathrm{ch}} = (r_{\mathrm{ch,ex}} - r_{\mathrm{ch,th}})/r_{\mathrm{ch,ex}}$, which have been obtained from the self-consistent HF calculations with these new Skyrme forces for a number of nuclei. As seen from Fig. 4, the found variants of the Skyrme forces reproduce the experimental data for binding energies within an accuracy of 1%, which is better than in the case of the variants of the standard-form Skyrme forces SkOP1 and SkOP2 found in Ref. [8], and the accuracy for charge radii is within 1.5%. Note also that for the difference $r_n - r_p$ of the neutron and proton radii of the ^{208}Pb nucleus, which is discussed in the literature, the new Skyrme-force variants SkOP3, SkOP4, SkOP5, and SkOP6 give the values 0.187, 0.192, 0.206, and 0.185 fm, respectively, which agree with the experimental value (see Ref. [27]). For the spin-orbit splitting of the neutron $3p$ level in the ^{208}Pb nucleus, which was controlled in the fitting, all these forces yield values of about 1 MeV, which is also close to the experimental value (see Ref. [1]).

It is also of interest to compare the single-particle spectra of nuclei obtained when using the found variants of the extended Skyrme forces with analogous spectra calculated on the basis of other known Skyrme forces as well as with experimental data. Such a comparison of the spectra is shown for the ^{208}Pb nucleus in Table III. Recall that the KDE0 force

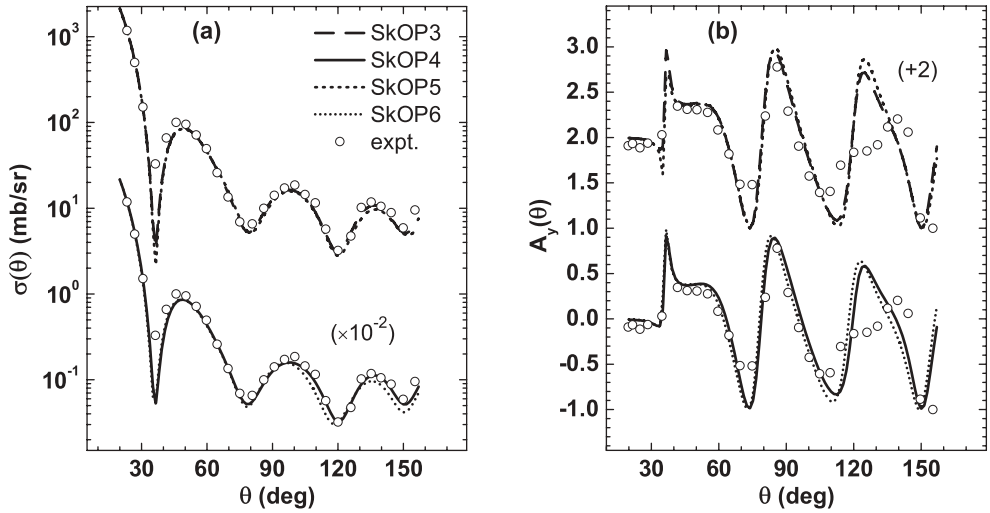

FIG. 3. Differential cross section $\sigma(\theta)$ (a) and analyzing power $A_y(\theta)$ (b) of the elastic scattering of 13.9-MeV neutrons on ^{120}Sn nuclei calculated with the found variants of extended Skyrme forces. The numbers in parentheses are the offsetting factor for the cross section and the offset value along the ordinate axis for the analyzing power.

has the standard form, whereas the BSk18 force is of the same form as in Eqs. (1)–(3). The single-particle spectra for these forces have been taken from the original papers (the calculations performed by us yield the same results). It is seen from Table III that the found extended-Skyrme-force variants describe the single-particle energies of the ^{208}Pb nuclei on the whole not worse than the *NN* forces obtained from fitting only characteristics of nuclear structure and nuclear matter. Moreover, our new *NN* forces improve the description of the neutron spectrum above the Fermi level as compared to the standard-form *NN* force KDE0 even to a greater extent than the extended force BSk18 does.

From fitting the extended-Skyrme-force parameters, we have obtained values (see Table II) of the main characteristics of symmetric nuclear matter E/A, ρ_0, m^*/m, J, κ, and K_v involved in the optimization procedure, which are close to the ones generally adopted at present in the literature (see, for example, a discussion of these quantities in Refs. [5,13,14]). Also, in Table II we present values of some other important characteristics of symmetric nuclear matter, which are discussed in the literature, namely, the slope L of the symmetry energy expansion in ρ at saturation density [see Eqs. (A24) and (A25) in Ref. [13]], the skewness coefficient K' in the third-order term of the energy-per-particle expansion in ρ in the vicinity of ρ_0 [see Eqs. (8a) and (9a) in Ref. [14]], as well as the Landau parameters G_0, G'_0, G_1, G'_1, F_0, F'_0, F_1, and F'_1 at the saturation density. As seen from Table II, the above-listed quantities have values that do not contradict the constraints usually imposed on them (see, for example, Refs. [5,14,28] and references therein). With the found *NN* forces, we have also performed calculations of the density dependence of the Landau parameters, which have shown that these quantities satisfy the usual requirement $G_l, G'_l, F_l, F'_l > -(2l+1)$ in the density region up to $3\rho_0$, except for the parameter F_0 at density values below about 0.1 fm^{-3}, which, however, is also characteristic of other known Skyrme forces (see Refs. [5,14]).

In Refs. [13,14], it was noted that the introduction of both the density- and momentum-dependent terms in the Skyrme

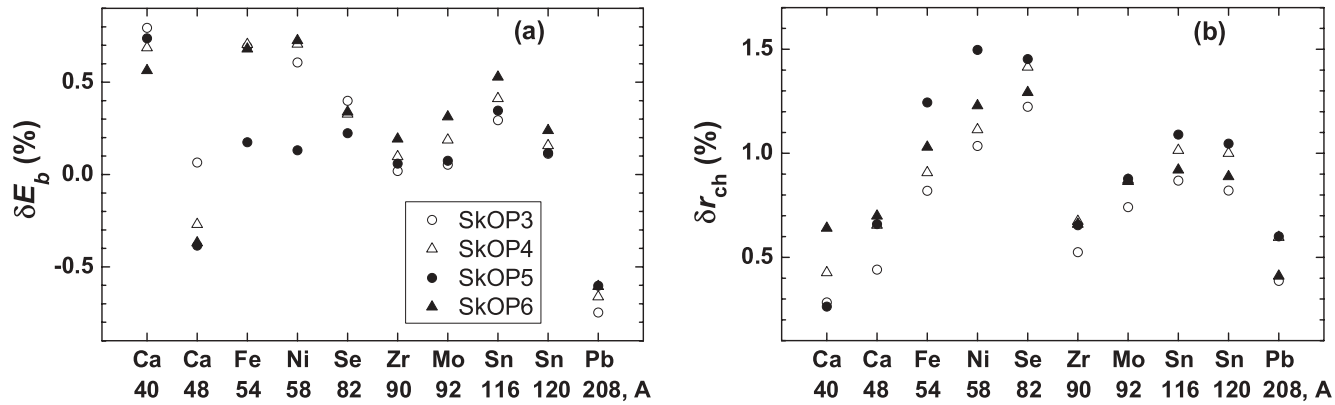

FIG. 4. Relative deviations δE_b (a) and $\delta r_{\rm ch}$ (b) of the binding energies and charge radii calculated with the found extended Skyrme forces from their experimental values for a number of nuclei.

TABLE III. Proton and neutron single-particle energies (MeV) for the nucleus ^{208}Pb calculated with different Skyrme forces. Experimental values are taken from Ref. [1]. The asterisk denotes the Fermi level.

Orbits	Expt.	KDE0	BSk18	SkOP3	SkOP4	SkOP5	SkOP6
				Protons			
$1g_{9/2}$	−15.43	−17.85	−16.3	−17.40	−17.01	−16.99	−16.87
$1g_{7/2}$	−11.43	−13.77	−13.0	−13.66	−13.37	−13.12	−13.23
$2d_{5/2}$	−9.70	−11.37	−10.2	−10.55	−10.05	−10.08	−9.75
$1h_{11/2}$	−9.37	−9.87	−8.8	−9.16	−8.70	−8.89	−8.44
$2d_{3/2}$	−8.38	−9.43	−8.4	−8.85	−8.35	−8.36	−8.06
$3s^*_{1/2}$	−8.03	−8.67	−7.7	−8.08	−7.53	−7.60	−7.30
$1h_{9/2}$	−3.77	−4.00	−4.0	−3.73	−3.39	−3.28	−3.11
$2f_{7/2}$	−2.87	−2.78	−2.2	−2.07	−1.47	−1.70	−1.23
				Neutrons			
$1h_{9/2}$	−10.85	−12.39	−12.6	−12.64	−13.12	−12.63	−13.65
$2f_{7/2}$	−9.72	−11.60	−11.6	−11.60	−11.89	−11.81	−12.05
$1i_{13/2}$	−9.01	−9.33	−9.4	−9.86	−10.10	−10.05	−10.29
$3p_{3/2}$	−8.27	−8.67	−8.8	−9.02	−9.27	−9.23	−9.46
$2f_{5/2}$	−7.95	−8.59	−8.8	−8.99	−9.29	−9.19	−9.46
$3p^*_{1/2}$	−7.38	−7.54	−7.7	−8.03	−8.28	−8.21	−8.47
$2g_{9/2}$	−3.94	−2.86	−3.5	−3.72	−3.87	−3.93	−3.96
$1i_{11/2}$	−3.15	−1.65	−2.7	−2.59	−2.94	−2.60	−3.19
$1j_{15/2}$	−2.53	−0.41	−1.2	−1.51	−1.61	−1.69	−1.73
$3d_{5/2}$	−2.36	−0.43	−1.2	−1.61	−1.76	−1.69	−1.90
$4s_{1/2}$	−1.91	0.08	−0.7	−1.05	−1.20	−1.05	−1.34
$2g_{7/2}$	−1.45	0.38	−0.4	−0.91	−1.10	−1.06	−1.21
$3d_{3/2}$	−1.42	0.56	−0.2	−0.63	−0.78	−0.65	−0.93

forces allows one to eliminate the ferromagnetic instability and its attendant collapse of pure neutron matter, which usually occur for Skyrme forces of the standard form [13], and specifically for the forces SkOP1 and SkOP2, which we obtained in Ref. [8]. In this connection, we have examined the density-dependence behavior of the energy per nucleon in pure neutron matter for the found variants of the extended Skyrme forces. For all four parameter sets SkOP3–SkOP6, we have observed the stability of neutron matter against a ferromagnetic transition at least at densities $\rho < 1$ fm^{-3}. As an example, in Fig. 5 we present the equation of state (EoS), E/A via ρ, for the unpolarized and completely polarized neutron matter for one of our parameter sets SkOP4 in comparison with the results of analogous calculations with the standard Skyrme force KDE0. In this figure, we also present the results of calculations for the realistic EoS V18 obtained in Ref. [29] for the unpolarized neutron matter. (In Ref. [14] this EoS was referred as LS2 and employed for obtaining the BSk21 force.) One can see that in the case of SkOP4 the unpolarized-state curve lies below the one for the polarized neutron matter in the whole density range, unlike the case of the KDE0 force, for which these curves cross each other, so that at sufficiently high densities, $\rho > 0.6$ fm^{-3}, the polarized state becomes the ground one. Note that the unpolarized-neutron-matter EoS for the SkOP4 force is close to the realistic EoS V18.

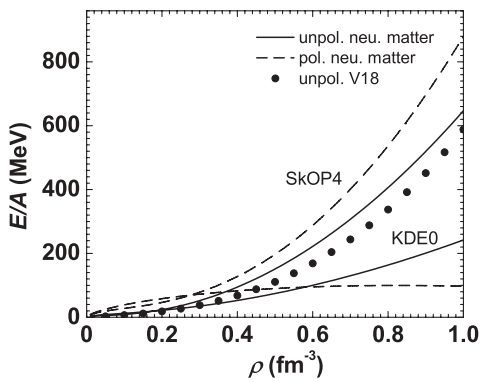

FIG. 5. Equations of state for the unpolarized and completely polarized neutron matter for the found force SkOP4 and for the standard force KDE0 [19]. Also shown is the realistic unpolarized-state EoS V18 [29].

Thus, it follows from the considered analysis that the extended Skyrme-force variants obtained in this work, along with a good description of the fitted observables for the considered case of the elastic neutron scattering, also quite satisfactorily reproduce a variety of parameters of symmetric nuclear and neutron matter, as well as the main characteristics of finite nuclei in a wide range of mass numbers.

IV. CALCULATIONS OF OBSERVABLES OF THE NEUTRON AND PROTON SCATTERING ON DIFFERENT NUCLEI

Further, we have employed the extended Skyrme-force variants SkOP3–SkOP6 found from the described optimization analysis of the differential cross section and analyzing power for the chosen case of $n + {}^{120}$Sn elastic scattering at 13.9 MeV,

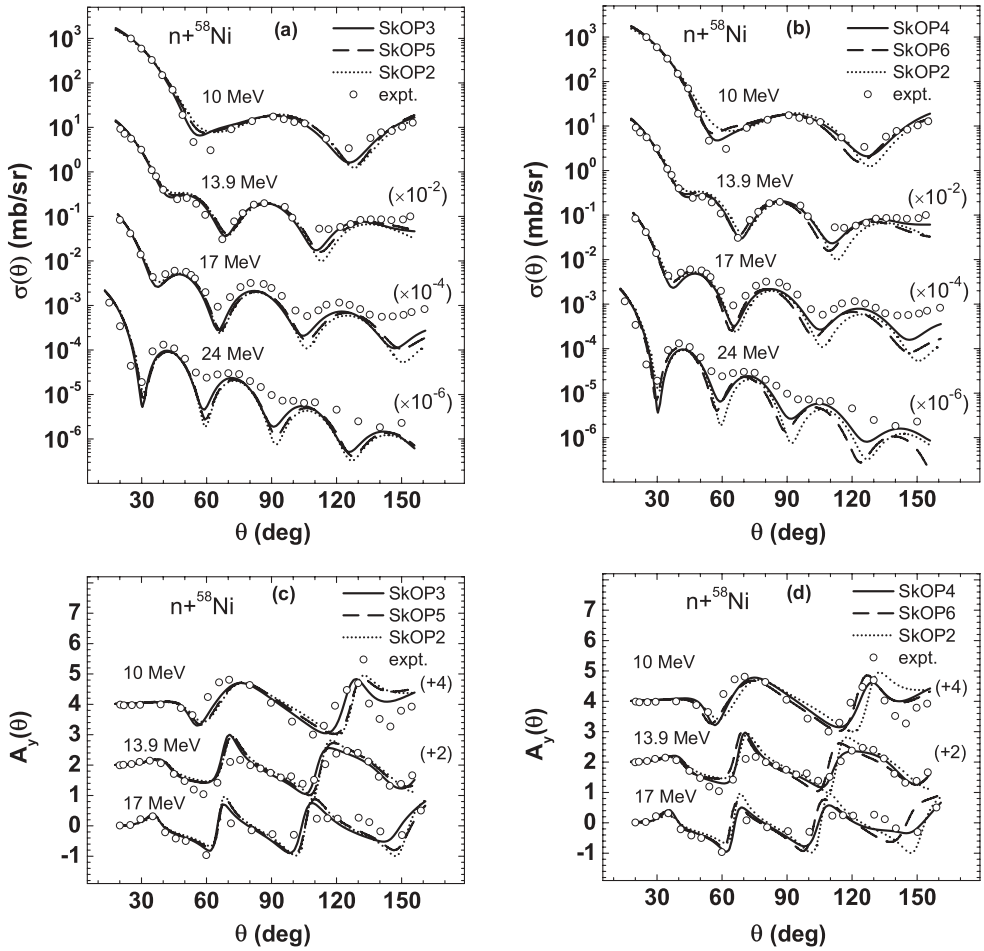

FIG. 6. Differential cross sections $\sigma(\theta)$ and analyzing powers $A_y(\theta)$ of the elastic neutron scattering on ^{58}Ni nuclei at different energies calculated with the found extended Skyrme-force variants SkOP3–SkOP6 and with the standard Skyrme force SkOP2 obtained in Ref. [8]. The numbers in parentheses are the offsetting factors for the cross sections and the ordinate-axis offset values for the analyzing powers. Experimental data are from Refs. [30–32].

to use them for describing scattering observables of the neutron and proton scattering on other target nuclei in a wide mass-number range and at other incident-nucleon energy values.[1]

In Figs. 6 and 7, we present examples of such calculations of differential cross sections and analyzing powers of the neutron scattering on ^{58}Ni and ^{208}Pb nuclei at several energy values. We compare these results with those obtained on the basis of the MOP model under consideration, but using the standard-form Skyrme force SkOP2, which was also found from a similar optimization analysis of the nA scattering earlier in Ref. [8]. It is seen from the figures that all new variants of *NN* forces give in general a satisfactory agreement with the experimental data on the neutron scattering on the target nuclei belonging to quite different regions of the mass-number range. Moreover, the found extended Skyrme forces provide a better description of all experimental cross sections and analyzing powers than the standard-form variant SkOP2 does. This improvement in the description of observables becomes more appreciable at higher incident energies. The agreement with experimental data worsens with an increase in incident energy, which is a consequence of a too rapid growth of the depth of the imaginary part of the MOP, as was discussed in detail in Ref. [8]. However, this worsening occurs more slowly for the extended Skyrme forces, which is well exemplified by the $n + {}^{208}$Pb scattering at 40 MeV. In this case, the calculation with the standard force SkOP2 yields too pronounced diffraction oscillations of the cross section, while the new extended Skyrme forces SkOP3 and SkOP4 provide a refraction damping of these oscillations, which resembles the experimentally observed behavior. These facts are caused by a slower increase of the depth of the imaginary part of the MOP with energy for the extended Skyrme forces as compared with SkOP2. Examination of the calculated MOP shows that the behavior of its imaginary part is mainly improved in the surface region owing to the contributions coming from the both density- and momentum-dependent terms of the *NN* forces. This is manifested especially well for the variants SkOP3 and SkOP4. It should be noted that these two variants give the best description of experimental data

[1]The experimental data on cross sections and analyzing powers were mainly taken from the electronic Experimental Nuclear Reaction Data at http://www-nds.iaea.org/exfor/exfor.htm.

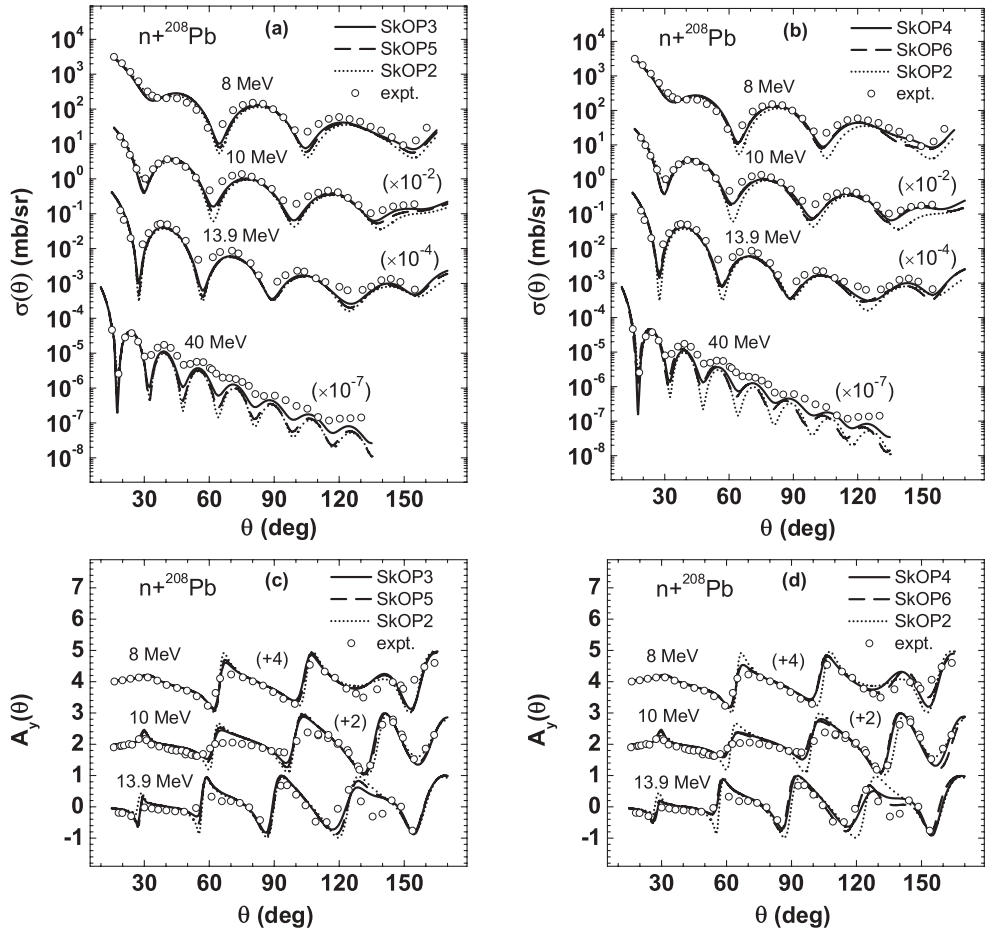

FIG. 7. The same as in Fig. 6, but for the neutron scattering on ^{208}Pb nuclei. Experimental data are from Refs. [33–37].

in all cases under consideration. Besides, the results obtained with SkOP3 and SkOP4 are fairly close to each other. For this reason, below we shall restrict ourselves to the consideration of calculations with only one of the new force variants, namely, SkOP4.

We have also applied the MOP model under consideration and the obtained variants of the Skyrme forces involving both the density- and momentum-dependent terms to calculations of the reaction and total interaction cross sections σ_r and σ_t, which are important integrated characteristics of the *NA* scattering. In Fig. 8, we present the calculated energy dependences of these cross sections for the neutron scattering on ^{90}Zr and ^{208}Pb nuclei for the chosen force variant SkOP4 in comparison with the results for our standard-form variant SkOP2. The

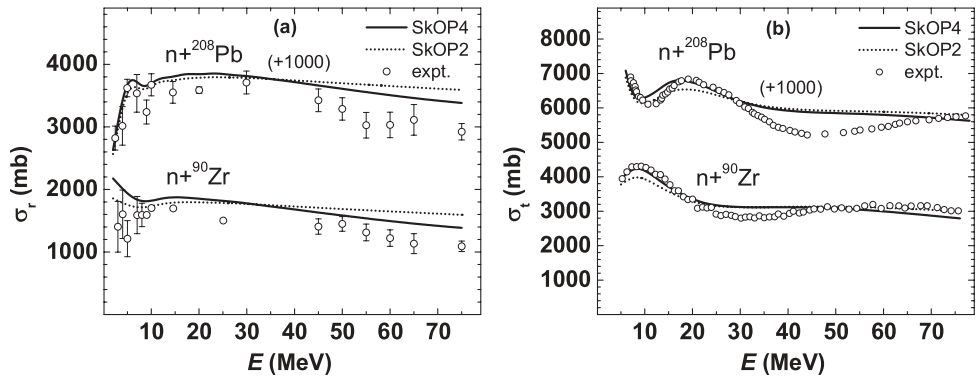

FIG. 8. Reaction cross sections σ_r (a) and total cross sections σ_t (b) for the neutron scattering on ^{90}Zr and ^{208}Pb nuclei as functions of the neutron energy E calculated with the extended force SkOP4 and the standard-form force SkOP2 from Ref. [8]. The numbers in parentheses are the ordinate-axis offset values. Experimental data are from Refs. [38–40].

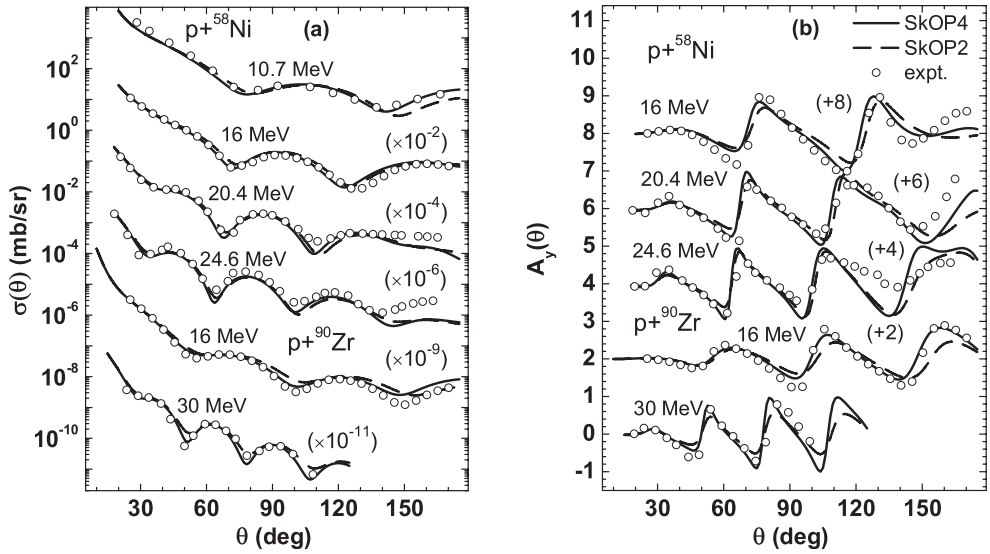

FIG. 9. Differential cross sections $\sigma(\theta)$ and analyzing powers $A_y(\theta)$ of the elastic proton scattering on ^{58}Ni and ^{90}Zr nuclei at different energies calculated with the new extended Skyrme force SkOP4 and with the standard-form force SkOP2 from Ref. [8]. The numbers in parentheses are the offsetting factors for the cross sections and the ordinate-axis offset values for the analyzing powers. Experimental data are from Refs. [41–44].

calculations with both SkOP2 and SkOP4 variants are in a reasonable agreement with the corresponding experimental data (the data for σ_r are for targets of natural isotopic composition). However, we may note that the extended Skyrme force SkOP4 provides a somewhat better description of the reaction cross sections in the region of higher neutron energies, as it also was in the case of differential cross sections of the elastic nA scattering.

As is distinct from Ref. [8], in which we considered the application of the MOP model of this type to describing the neutron scattering only, in this work we have additionally performed calculations of observables of the proton scattering on various target nuclei in a wide range of mass numbers and in a rather wide region of incident energies, using both the new variants of the extended Skyrme forces and the standard-form variants SkOP1 and SkOP2. The performed analysis has shown that, just like it was in the case of the neutron scattering, the MOP model under consideration allows us to obtain a satisfactory description of experimental data on the pA scattering. Besides, it should be noted that the SkOP3 force again gives results close to those for the SkOP4 force, and the results for SkOP1 are close to those for the SkOP2 force. As an example, in Figs. 9 and 10 we show results of some such calculations of the differential cross sections and analyzing powers for the elastic proton scattering on ^{58}Ni, ^{90}Zr, ^{120}Sn, and ^{208}Pb nuclei while making use of two chosen

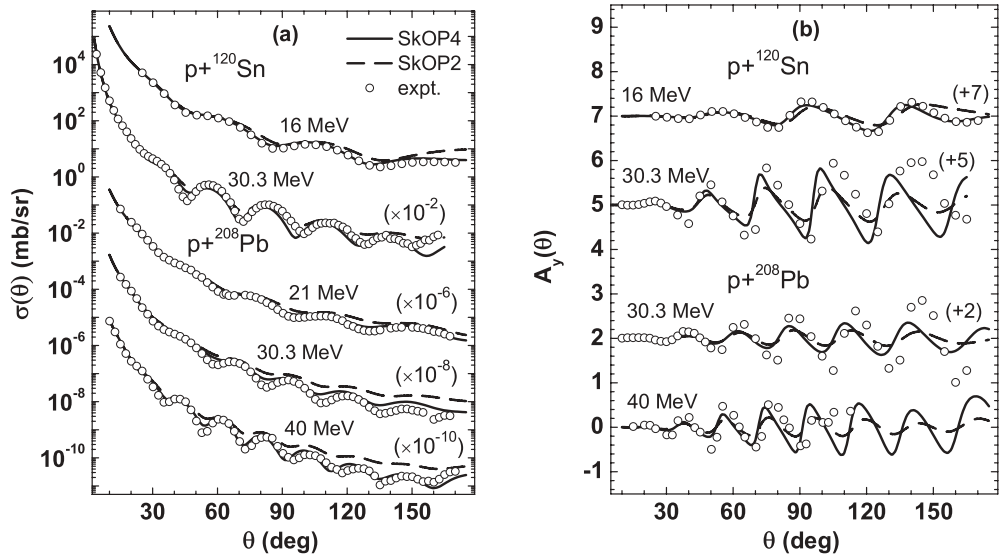

FIG. 10. The same as in Fig. 9, but for the proton scattering on ^{120}Sn and ^{208}Pb. Experimental data are from Refs. [42,45–48].

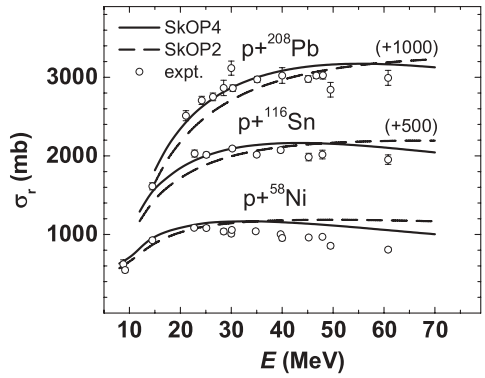

FIG. 11. Reaction cross sections σ_r for the proton interaction with ^{58}Ni, ^{116}Sn, and ^{208}Pb nuclei as functions of the proton energy E for the new extended force variant SkOP4 and the standard-form variant SkOP2 from Ref. [8]. The numbers in parentheses are the ordinate-axis offset values.

variants of the Skyrme forces: the extended SkOP4 force and the standard-form SkOP2 force. As can be seen from Figs. 9 and 10, the new Skyrme force SkOP4 gives a good agreement of the calculated observables for the proton scattering on various nuclei with the corresponding experimental data, significantly improving the description of both the angular and energy dependence of these quantities as compared to the results of calculations with the standard-form *NN* force SkOP2. The improvement of the description of the energy dependence of pA scattering observables on the basis of the MOP model under consideration while making use of the extended Skyrme forces is also confirmed by the calculations of the total cross sections of pA reactions, which we have performed in a rather wide range of the incident proton energies. Examples of such calculations with the SkOP4 and SkOP2 forces for the ^{58}Ni, ^{116}Sn, and ^{208}Pb target nuclei are shown in Fig. 11. As in the case of the neutron scattering, the results of calculations of $\sigma_r(E)$ with the SkOP4 force are in better agreement with the experimental data from Ref. [49].

V. CONCLUSION

We have considered a model of the *NA* microscopic optical potential, in which the latter is obtained from calculations of the one-particle Green function mass operator making use of the extended variant of Skyrme forces that involves terms depending on both the density and momentum of the interacting nucleons. This model has been employed for searching for values of the parameters of the *NN* forces of this type on the basis of the optimization procedure proposed by the authors. This procedure includes an analysis of certain chosen angular distributions of the cross section and analyzing power of the elastic neutron scattering by nuclei with the simultaneous control of the main parameters of nuclear matter (the binding energy per nucleon, the equilibrium density, the symmetry energy, the isoscalar and isovector effective nucleon masses, and the incompressibility coefficient of nuclear matter). When performing specific calculations, we have fixed upon fitting the observables of the 13.9-MeV neutron scattering on ^{120}Sn nuclei. During the fitting, we also controlled the binding energies and charge radii for the target nucleus and two additional nuclei belonging to different regions the mass-number range, namely, the ^{40}Ca and ^{208}Pb nuclei, as well as the spin-orbit splitting of the neutron $3p$ levels of the ^{208}Pb nucleus.

Basing on this optimization procedure, we have found a number of parameter sets of the extended Skyrme forces involving both the density- and momentum-dependent terms for different values of the density exponents. These new variants of *NN* forces significantly improve the description of the analyzed scattering observables as compared with the results of calculations both with the Skyrme forces known from the literature (including the extended ones of the same type) and with the standard-form forces obtained by us in the previous work of Ref. [8] on the basis of the optimization analysis of an nA scattering cross section. The found new variants of the extended Skyrme forces provide a satisfactory description of the main characteristics of even-even nuclei. These forces also yield values of the main parameters of symmetric nuclear matter close to those generally adopted at present in the literature. This is the case both for the parameters involved in the optimization procedure and for a number of parameters that were not controlled during the fitting. In contrast to many standard-form *NN* forces, for all found variants of the extended Skyrme forces, the stability of pure neutron matter against a ferromagnetic transition is observed in a wide range of neutron densities.

The performed calculations also show that this model of the *NA* MOP based on the new variants of extended Skyrme forces yields a good description of differential cross sections and analyzing powers of the elastic scattering of both neutrons and protons on various target nuclei in a wide range of mass numbers at different incident nucleon energies. In all considered cases, there is observed a better agreement with the corresponding experimental data in comparison with results obtained with the standard-form *NN* Skyrme forces, especially at higher incident energies. The same situation takes place also in calculations of the cross sections of nA and pA reactions and of the total nA interaction cross sections. However, it should be stressed that, as was in our previous work (see Ref. [8]), certain problems in the description of the *NA* scattering observables arise when the incident energy increases, which are caused by a too rapid increase of the depth of the imaginary part of the MOP. At sufficiently high energy values, these problems cannot be eliminated by using the extended variant of Skyrme forces, and therefore, a further refinement of the model of the imaginary part of the MOP is required.

[1] D. Vautherin and D. M. Brink, Phys. Rev. C **5**, 626 (1972).
[2] T. H. R. Skyrme, Nucl. Phys. **9**, 615 (1959).
[3] M. Bender, P.-H. Heenen, and P.-G. Reinhard, Rev. Mod. Phys. **75**, 121 (2003).
[4] J. Stone and P.-G. Reinhard, Prog. Part. Nucl. Phys. **58**, 587 (2007).
[5] M. Dutra, O. Lourenço, J. S. Sá Martins, A. Delfino, J. R. Stone, and P. D. Stevenson, Phys. Rev. C **85**, 035201 (2012).

[6] V. V. Pilipenko, V. I. Kuprikov, and A. P. Soznik, Int. J. Mod. Phys. E **18**, 1845 (2009).
[7] V. I. Kuprikov, V. V. Pilipenko, A. P. Soznik, V. N. Tarasov, and N. A. Shlyakhov, Phys. At. Nucl. **72**, 975 (2009).
[8] V. V. Pilipenko, V. I. Kuprikov, and A. P. Soznik, Phys. Rev. C **81**, 044614 (2010).
[9] Q. Shen, J. Zhang, Y. Tian, Z. Ma, and Y. Zhuo, Z. Phys. A **303**, 69 (1981).
[10] Q.-b. Shen, Y.-l. Han, and H.-r. Guo, Phys. Rev. C **80**, 024604 (2009).
[11] S. Krewald, V. Klemt, J. Speth, and A. Faessler, Nucl. Phys. A **281**, 166 (1977).
[12] M. Farine, J. M. Pearson, and E. Tondeur, Nucl. Phys. A **615**, 135 (1997).
[13] N. Chamel, S. Goriely, and J. M. Pearson, Phys. Rev. C **80**, 065804 (2009).
[14] S. Goriely, N. Chamel, and J. M. Pearson, Phys. Rev. C **82**, 035804 (2010).
[15] K.-F. Liu, H. Luo, Z. Ma, Q. Shen, and S. A. Moszkowski, Nucl. Phys. A **534**, 1 (1991).
[16] C. B. Dover and N. Van Giai, Nucl. Phys. A **190**, 373 (1972).
[17] V. Yu. Gonchar, E. V. Inopin, and V. I. Kuprikov, Sov. J. Nucl. Phys. **25**, 25 (1977).
[18] V. E. Mitroshin, Phys. At. Nucl. **68**, 1314 (2005).
[19] B. K. Agrawal, S. Shlomo, and V. K. Au, Phys. Rev. C **72**, 014310 (2005).
[20] P. Klüpfel, P.-G. Reinhard, T. J. Bürvenich, and J. A. Maruhn, Phys. Rev. C **79**, 034310 (2009).
[21] P. P. Guss, R. C. Byrd, C. R. Howell, R. S. Pedroni, G. Tungate, R. L. Walter, and J. P. Delaroche, Phys. Rev. C **39**, 405 (1989).
[22] H. Chandra and G. Sauer, Phys. Rev. C **13**, 245 (1976).
[23] V. I. Kuprikov, A. P. Soznik, A. A. Khomich, and N. G. Shevchenko, Ukr. Fiz. Zh. **32**, 1297 (1987).
[24] W. Bertozzi, J. Friar, J. Heisenberg, and J. W. Negele, Phys. Lett. B **41**, 408 (1972).
[25] R. B. Firestone, *Table of Isotopes*, 8th ed. (Wiley, New York, 1996).
[26] I. Angeli, At. Data Nucl. Data Tables **87**, 185 (2004).
[27] J. Piekarewicz, B. K. Agrawal, G. Colò, W. Nazarewicz, N. Paar, P.-G. Reinhard, X. Roca-Maza, and D. Vretenar, Phys. Rev. C **85**, 041302(R) (2012).
[28] P. Möller, W. D. Myers, H. Sagawa, and S. Yoshida, Phys. Rev. Lett. **108**, 052501 (2012).
[29] Z. H. Li and H.-J. Schulze, Phys. Rev. C **78**, 028801 (2008).
[30] P. P. Guss, R. C. Byrd, C. E. Floyd, C. R. Howell, K. Murphy, G. Tungate, R. S. Pedroni, R. L. Walter, J. P. Delaroche, and T. B. Clegg, Nucl. Phys. A **438**, 187 (1985).
[31] R. S. Pedroni, C. R. Howell, G. M. Honore, H. G. Pfutzner, R. C. Byrd, R. L. Walter, and J. P. Delaroche, Phys. Rev. C **38**, 2052 (1988).
[32] Y. Yamanouti, J. Rapaport, S. M. Grimes, V. Kulkarni, R. W. Finlay, D. Bainum, P. Grabmayr, and G. Randers-Pehrson, in *Nuclear Cross Sections for Technology, Proceedings of the International Conference, Knoxville, Tennessee, 1979*, edited by J. L. Fowler, C. H. Johnson, and C. D. Bowman (US Dept. of Commerce, National Bureau of Standards, Washington, DC, 1980), p. 146.
[33] M. L. Roberts, P. D. Felsher, G. J. Weisel, Zemin Chen, C. R. Howell, W. Tornow, R. L. Walter, and D. J. Horen, Phys. Rev. C **44**, 2006 (1991).
[34] J. P. Delaroche, C. E. Floyd, P. P. Guss, R. C. Byrd, K. Murphy, G. Tungate, and R. L. Walter, Phys. Rev. C **28**, 1410 (1983).
[35] C. E. Floyd, Jr., Ph.D. thesis, Duke University, 1981.
[36] C. E. Floyd, P. P. Guss, K. Murphy, C. R. Howell, R. C. Byrd, G. Tungate, S. A. Wender, R. L. Walter, and T. B. Clegg, Phys. Rev. C **25**, 1682 (1982).
[37] R. P. DeVito, D. T. Khoa, S. M. Austin, U. E. P. Berg, and B. M. Loc, Phys. Rev. C **85**, 024619 (2012).
[38] J. Rapaport, V. Kulkarni, and R. W. Finlay, Nucl. Phys. A **330**, 15 (1979).
[39] M. Ibaraki, M. Baba, T. Miura, T. Aoki, T. Hiroishi, H. Nakashima, S.-I. Meigo, and S. Tanaka, J. Nucl. Sci. Technol. Suppl. **2**, 405 (2002).
[40] R. W. Finlay, W. P. Abfalterer, G. Fink, E. Montei, T. Adami, P. W. Lisowski, G. L. Morgan, and R. C. Haight, Phys. Rev. C **47**, 237 (1993).
[41] S. Kobayashi, K. Matsuda, Y. Nagahara, Y. Oda, and N. Yamamuro, J. Phys. Soc. Jpn. **15**, 1151 (1960).
[42] R. L. Varner, W. J. Thompson, T. L. McAbee, E. J. Ludwig, and T. B. Clegg, Phys. Rep. **201**, 57 (1991).
[43] P. J. van Hall, J. P. M. G. Melssen, S. D. Wassenaar, O. J. Poppema, S. S. Klein, and G. J. Nijgh, Nucl. Phys. A **291**, 63 (1977).
[44] R. de Swiniarski, D.-L. Pham, and G. Bagieu, Can. J. Phys. **55**, 43 (1977).
[45] B. W. Ridley and J. F. Turner, Nucl. Phys. **58**, 497 (1964).
[46] G. W. Greenlees, V. Hnizdo, O. Karban, J. Lowe, and W. Makofske, Phys. Rev. C **2**, 1063 (1970).
[47] W. T. H. van Oers, H. Haw, N. E. Davison, A. Ingemarsson, B. Fagerström, and G. Tibell, Phys. Rev. C **10**, 307 (1974).
[48] L. N. Blumberg, E. E. Gross, A. van der Woude, A. Zucker, and R. H. Bassel, Phys. Rev. **147**, 812 (1966).
[49] R. F. Carlson, At. Data Nucl. Data Tables **63**, 93 (1996).